A Study on Shunt Resistor-based Current Measurements for Fast Switching GaN Devices

Thilini Wickramasinghe, Bruno Allard, Cyril Buttay, Charles Joubert, Christian Martin, Jean-Fraçois Mogniotte, Hervé Morel, Pascal Bevilacqua, Thanh-Long Le, Stephane Azzopardi

A Study on Shunt Resistor-based Current Measurements for Fast Switching GaN Devices

Thilini Wickramasinghe[1], Bruno Allard[1], Cyril Buttay[1], Charles Joubert[1], Christian Martin[1]
Jean-Fraçois Mogniotte[1], Herve Morel[1], Pascal Bevilacqua[1], Thanh-Long Le[2], Stephane Azzopardi[2]
[1]Univ Lyon, Universite Claude Bernard Lyon 1, INSA Lyon, CNRS, Ampere, F-69621, Villeurbanne, France.
[2]Electrical & Electronics Division, Safran Tech - Safran Paris Saclay, France.
thilini.wickramasinghe@insa-lyon.fr

***Abstract*—Current viewing resistor (CVR) based measurement of a high frequency switching cell is presented. The drain current of the low-side GaN HEMT switch was measured at 100 kHz switching frequency for a maximum load current of 8 A and a dc input of 80 V. To analyze the results, both simulations and experiments were used. The parasitic elements of the PCB layout (i.e. calculated using the Ansys-Q3D Extractor software) were included in the simulation model. This paper explains the consequences of mounting CVRs in the common-source path of transistors compared to a circuit without a CVR. Simulation results are found to be in very good agreement with measurements. Hence, the simulation model can be used to estimate the current waveforms when it is not desirable to resort to intrusive measurement methods.**

***Index Terms*—CVR, GaN HEMT, high frequency, current measurements**

I. Introduction

Wide bandgap semiconductor materials enable power transistors to operate at high frequencies, high voltages and at high temperatures. In particular, Gallium Nitride (GaN) is attractive to build high electron-mobility transistors (HEMTs). They offer higher power density and lower on-resistance over silicon based counterparts. Therefore, lower losses are expected with a favourable impact on the heat dissipation strategy with a gain in mass. Due to a relatively stable threshold voltage over the range of 25° to 150° C and the positive temperature coefficient of the on-resistance, GaN HEMTs are more desirable for parallel configurations. However, a slight mismatch in the threshold voltage from one device to another may degrade the current distribution during switching. These circumstances are especially concerning as the GaN HEMTs have very fast switching times (with few tens of nanoseconds) and large oscillations may arise during transients.

To apply them in practical situations, it is important to examine the switching behaviour in order to identify and control these high current-voltage transients. However, these current waveforms are particularly difficult to measure without disturbing the behaviour of the circuit.

There are many current measuring concepts based on some basic physical principles [1], [2]. Most of the novel sensors are incorporated with digital signal processing technologies to achieve greater noise immunity and stringent design constraints of a printed circuit board (PCB).

Primarily, the current sensor (CS) techniques are based on;

- Shunt resistor-based transducers [3]– [5].
- Magnetic induction-based transducers (Rogowski coils, current transformers) [8]– [9].
- Magnetic-field based transducers (Hall effect, flux gate, magnetoresistive—MR) [10].

In general, shunt resistor-based CSs (SR-CS) are simple, highly linear and cost effective but they do not provide galvanic isolation [3]– [5]; whereas magnetic induction or field-based CSs are galvanically isolated [8]– [10]. However, compared to high-performance SR-CS (such as coaxial shunts) the bandwidth of Rogowski coil CSs is 10–100 times smaller and they introduce delays. Furthermore, the Rogowski coils cannot sense DC or low frequency currents.

Transformer-based CSs are applicable only for AC or high frequency pulse current. Planar transformers with high power are available for on-board integration [11], however, they are physically larger than other CSs.

Compared to the SR-CSs, the hall effect sensors and the fluxgate suffer from imperfections due to offset and gain drift under temperature. The dynamic response of a magnetoresistive (MR) CS is faster than a hall-based alternative sensor. However, it requires specific layout in designing primary bus bar to measure MR-based current, which is challenging in a compact design [12].

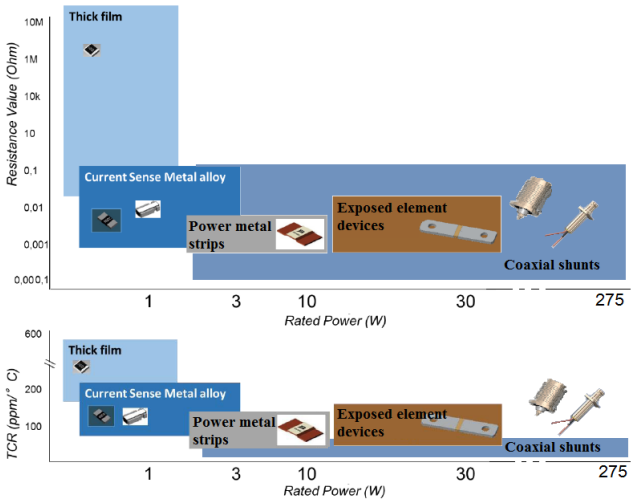

Fig. 1. A comparison of shunt resistor technologies (adapted from [4])

Figure 1 illustrates some commonly used CS resistor types with a comparison of the rated power against both resistor value and temperature coefficient [4]. As illustrated in Fig. 1, metal strips, high power exposed element-based devices and coaxial shunts resistors exhibit better temperature coefficient than that of a current sense metal alloy. However, the high power resistors are larger than the current sense metal alloy and they have parasitic inductances in the order of tens of nanohenries. Materials with high density (high thermal capacity and low specific heat) reduce the size of the resistor and are suitable for compact applications.

The coaxial shunts (also known as current viewing resistors—CVR) are suitable for high-frequency measurements despite of the constraints in their continuous operations that can cause thermal issues, and relatively large dimensions. They have extremely flat frequency response from DC to 2 GHz, present high performance in rise time and in accuracy. The CVRs are noise immune and have fast response for high current measurements (e.g. 5 kA with a 20 ns rise time) [6]. They have no offset and do not require an auxiliary power supply.

This paper presents a study on current measurements of a high frequency GaN device using a CVR. An experiment-based analysis was conducted to investigate the impact of mounting a shunt resistor in the power commutation path. For further evaluations, a simulation model of the circuit was used. The Section II describes about a coaxial shunt resistor-based current sensor followed by basic configurations of a test prototype. The experiment setup, test conditions and the experimental results are detailed in Section III. In Section IV, an analysis of the experiment and simulation results are presented. Practical issues and suggestions to address those issues are described in Section V with a conclusion.

II. Current Viewing Shunt Resistor-Based Measurements

Illustrated in Fig. 2(a) is a simplified equivalent circuit of a shunt resistor. Here, R_{cs} is the rated resistance while r_s and L_s are parasitic resistance and inductance respectively. The parasitic inductance in the CVR limits the operation bandwidth. To minimize the uncertainty of the resistor value, the voltage across the CVR is measured by Kelvin bridge connections.

Selection of an appropriate power rating of a resistor is made according to its joule losses (I^2R, where I is the maximum continuous current requirement of the application and R is nominal resistance). To reduce power dissipation, smaller resistor values are preferred. Shunt resistors with very low inductance or CVRs are being used in high frequency applications [5].

For this study, a lead connection type CVR with 25 mΩ resistance [15] shown in Fig. 2 was used. A 2.5 W capable CVR is sufficient for a case of maximum current of 10 A. The impedance measurement of the CVR (i.e. SDN-414-025 from TandM Research) in Fig. 3 depicts a low inductance in the device with short length, approximately 6.6 nH at high frequency range.

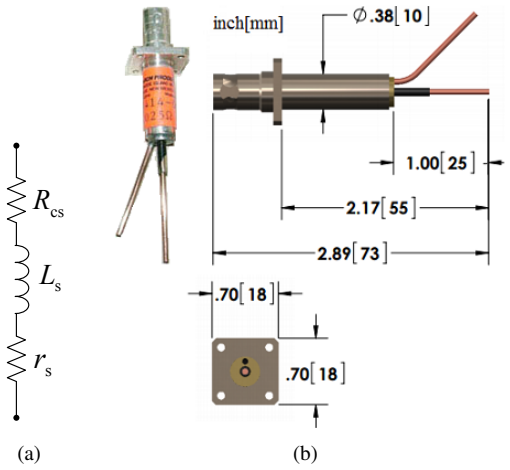

Fig. 2. CVR: (a) simplified circuit model of CVR, (b) SDN-414-025 from TandM Research [15].

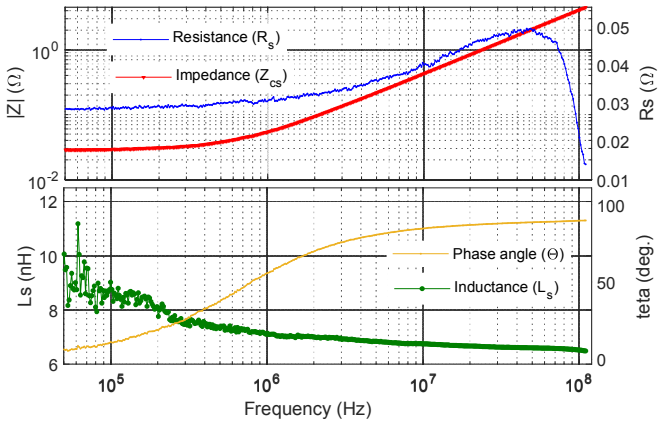

Fig. 3. Frequency response of SDN-414-025 from TandM Research, measured by 4294A precision impedance analyzer.

A. An overview and the experimental prototype

The main objectives of the experiment are to obtain CVR-based current measurements at high frequency operation and to observe the effect of inserting a CVR in the power path. To achieve them, two test cases are considered: *case 1*– prototype with the CVR and *case 2*– CVR unmounted prototype. A comparison of the voltage and current waveforms of the two cases can be used to observe the deviations. For the *case 2*, the current measurements can be predicted by a simulation model. Therefore, a precise model is essential for reliability of the study. This can be validated by replicating the experiment results.

The basic configuration of the test circuit is a half-bridge converter built with a GaN HEMT as the low-side switch and a Schottky diode in the high-side. Figure 4 illustrates a schematic diagram of the prototype with the CVR. For non-isolated probe measurements, the best position is to mount

TABLE I
LIST OF MAIN COMPONENTS

Function	Component	Manufacturer	Description
Low side switch	GS66516T	GaN Systems inc.	650 V, 60 A, 27 mΩ
High side switch	IDH16G120CS	Infineon	40 A, 80 V/ns
Gate driver	UCC27611DRV	Texas Instruments	5 V_{out}, 4–6 A
Iso. power supply of the gate driver	MEJ1S1205SC	Murata	5 V, 200 mA, 1 W, 5.2 kVdc isolation
Fiber optics receiver	HFBR-2521Z1	Broadcom	Links at dc-5 MBd
Bulk capacitors	EEVEB2C100Q	Panasonic	10μF±20%, 160Vdc, Al. Elect.
Filter capacitors	CKG57K	TDK single layer	2.2μF ±20% 450Vdc, Ceramic
Current sensor	SDN-414-025	T&M Research	25 mΩ ± 4%, 2 W, 1200 Mhz

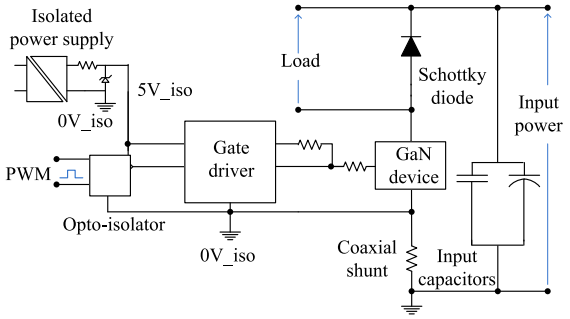

Fig. 4. Schematic diagram of the test prototype

the CVR in the source path. As shown in Fig. 4 the current sensor was implemented between the source terminal and the common ground that reduce the complexity of having a ground-referenced signal.

The output characteristics of the gate driver controls the switching behaviour of the GaN HEMT. By adjusting the gate resistance, on-off transient speeds of the switch can be changed. The pulse width modulated (PWM) signal is supplied through a fiber optics receiver to provide isolation. A capacitor bank is used for decoupling during high current transient. Two 10 μF electrolytic capacitors and six 2.2 μF ceramic capacitors were implemented for decoupling. The key components of the experimental prototype are listed in Table I.

III. EXPERIMENTAL SETUP AND RESULTS

A. Test setup and conditions

The main testing apparatus used in the setup are digital oscilloscope (Tektronix DPO 4034B, 350 MHz) combines with passive voltage probes (Tektronix P6139B, 500 Mhz), a current probe (TCP0030A , dc to >120MHz, 30 A—maximum range), a differential probe (EDITEST GE-8115, 30 MHz bandwidth), and an arbitrary signal generator (DG645 digital delay/pulse generator for PWM generation). For the case of CVR measurements, a BNC cable was used. The EDITEST GE-8115 probe was used to verify the differential voltages obtained by two passive probes.

In general, the prototypes were tested under the conditions that are summarized in Table II. The results presented in the paper are based on an input voltage of 80 V and a maximum load of ∼8 A. The load is a solenoid made with 17 turns wound around a polyvinyl-chloride tube with 5 cm diameter. Its model corresponds to a 10 μH inductor in series with a 260 mΩ resistor and the bandwidth of 42.5 MHz which in agreement with measured values as shown in Fig. 5.

TABLE II
TEST CONDITIONS

Parameters	Minimum	Nominal	Maximum
Input voltage	10 V	25 V	80 V
Load		7 A	10 A
Switching frequency	100 kHz	200 kHz	400 kHz
Pulse width		250 ns	500 ns
No. of bursts		10	
Pulse frequency		10 Hz	10 kHz

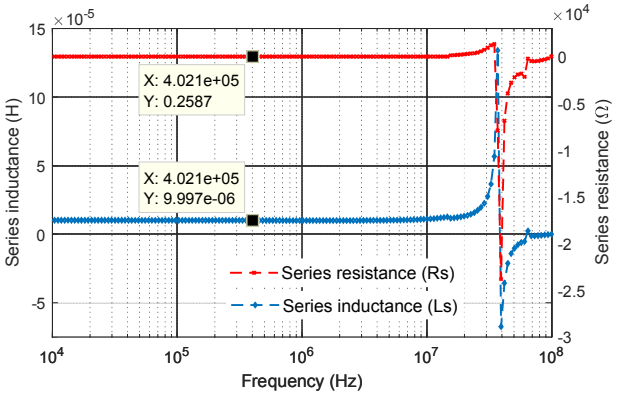

Fig. 5. Frequency response of the load

A repetitive pulse test setup was used to evaluate the switching performance of the GaN device. In the operation of the circuit, a set of discrete pulse is fed to the gate at a repetition rate of 1 kHz to avoid self heating of the GaN device. There were 10 pulses per set, each with 250 ns pulse width and 10 μs pulse period. This corresponds to a 100 kHz switching frequency with 2.5% duty cycle. The oscilloscope is triggered at the 10^{th} pulse of the set to obtain the measurements.

B. Test results

Figure 6(a) illustrates the *case 1* configuration of the CVR mounted printed circuit board (PCB). To avoid adding more parasitics to the circuit, the leads of the CVR connectors were kept short. In the experiment setup, a heat sink was mounted to prevent overheating of the Schottky diode. The measured voltage across the resistor is shown in Fig. 6(b) which was

used to estimate drain current. As seen in the figure, the estimated drain current (current via CVR) with respect to drain voltage and load current was obtained.

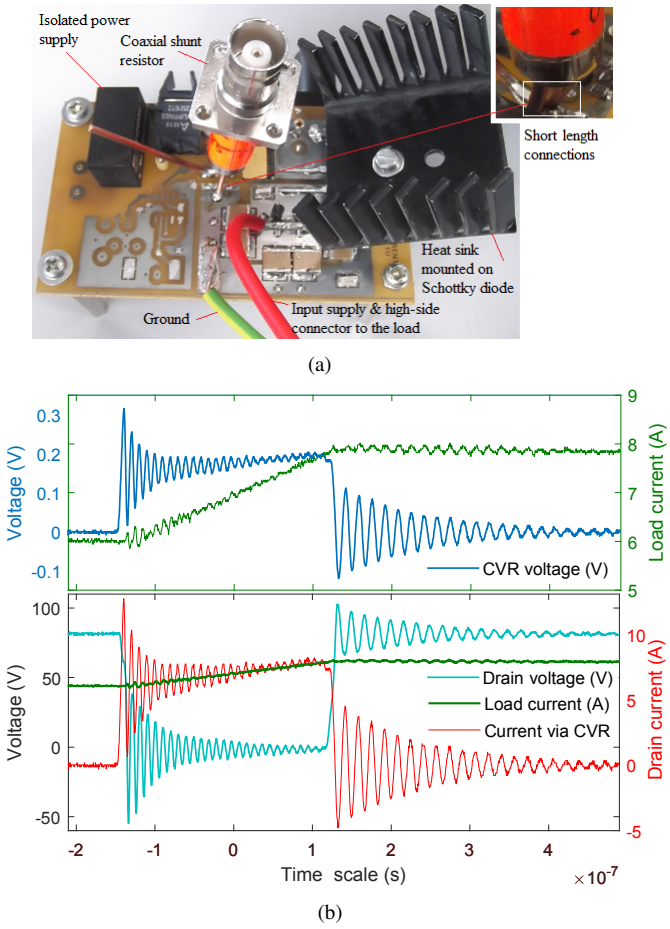

Fig. 6. *Case 1*: (a) Experimental prototype with current sensing via coaxial shunt resistor. (b) CVR-based measurements during transients. Input voltage is at 80 V.

In order to investigate the effect of adding shunt resistor in the power rail, the CVR was removed from the PCB. A copper strip was used to connect source and the ground as shown in Fig. 7(a) and no drain current can be measured in this configuration. Figure. 7(b) illustrates experimental results acquired from the PCB.

The drain voltages of the two cases can be compared as illustrated in Fig. 8. The results depicts that the coaxial shunt has a clear influence on the drain to source voltage. Indeed, the coaxial shunt resistor introduces parasitic inductance in the circuit due to its connecting leads. Further, it explains the lower frequency of the ringing compared to the *case 2*. However, to compare the drain current waveforms in the two cases, it is required to obtain the drain current waveform of the *case 2*. This can be achieved using a simulation model.

IV. Simulation Model of Circuit for the Validation of Experiment Results

The aim of the simulation is to replicate experimental results of the *case 2* in order to predict the drain current

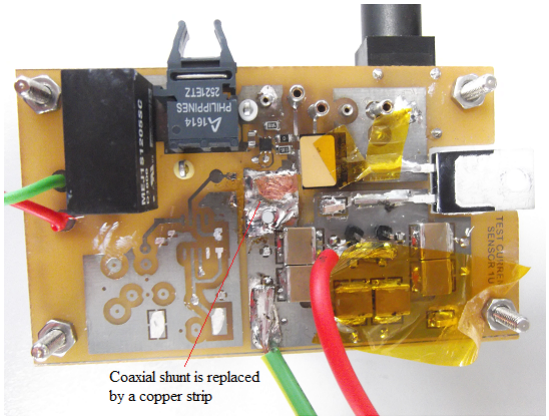

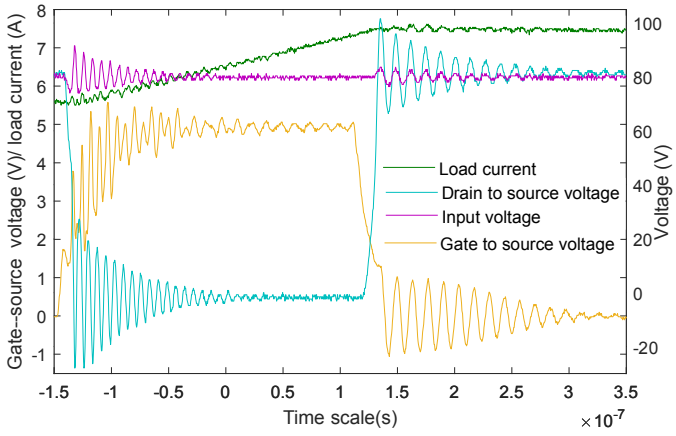

Fig. 7. *Case 2*: (a) prototype without current sensor, (b) experimental results of voltage-current of PCB without the CVR

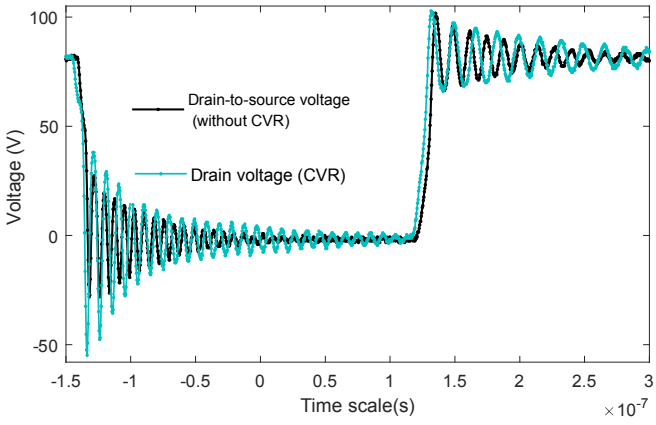

Fig. 8. A comparison of drain voltages of the two PCBs with and without CVR mounted in the power path.

waveform. Further, a model with an ideal layout can be used to compare the parasitic effect of PCB traces. A SPICE-based simulation meta-model was designed based on the simplified circuit diagram with the key components. The manufacturer-supplied SPICE models of the GaN HEMT, the Schottky diode and the gate driver were used. The load was represented by

an inductor connected in parallel with a parasitic capacitor. Further, the parasitic elements of the decoupling capacitors were included to their models.

For the extraction of the PCB layout parasitics, the Ansys-Q3D software was used. Figure 9(a) illustrates the simplified diagram of the parasitic components considered for this case. In this circuit, both power and the control commutation paths are in the same side of a single layer configuration. The parasitics between the gate and gate-driver output is insignificant due the compact design as seen in Fig 9(b). Therefore, the parasitics in this path can be neglected.

The values of parasitic components corresponding to the PCB traces were calculated using Ansis-Q3D software. They were included in the SPICE meta-model as seen in Fig. 10. For better fitting with the experiment curves, some of these values were slightly adjusted. The estimated resistance of the copper strip used in *case 2* is approximately 0.15 mΩ, where the length, thickness and the width are respectively 11 mm, 5 mm and 0.254 mm.

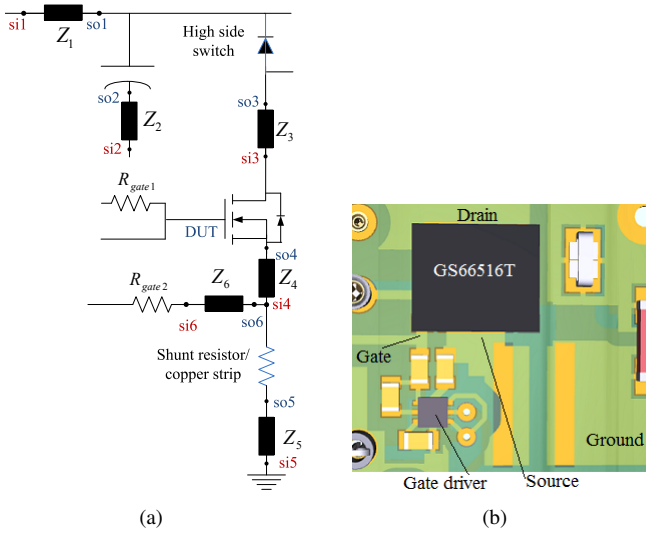

Fig. 9. Consideration of parasitic components: (a) simplified circuit model with consideration of parasitics in the layout, (b) the GaN HEMT and driver on the PCB.

The simulation results of the *case 2* are compared with its experiments as shown in Fig. 11. The inclusion of stray capacitors of the PCB (i.e. C_{x1}, C_{x2} and C_{x3}) made the simulation results more comparable to its experiments. The outcome of the approach indicates that the simulation results during transients are in fair agreement with its experiments to predict the drain current waveform.

The manufacturer provides three different models for GS66516T HEMT [16]. The basic model represents the electrical characteristics while the second and the third models are comprised with thermal characteristics, and stray inductances respectively. All three models were studied by comparing the results of simulations with the experiments. For this application, there was no substantial difference in the outcome provided that the absent device parasitics are incorporated externally.

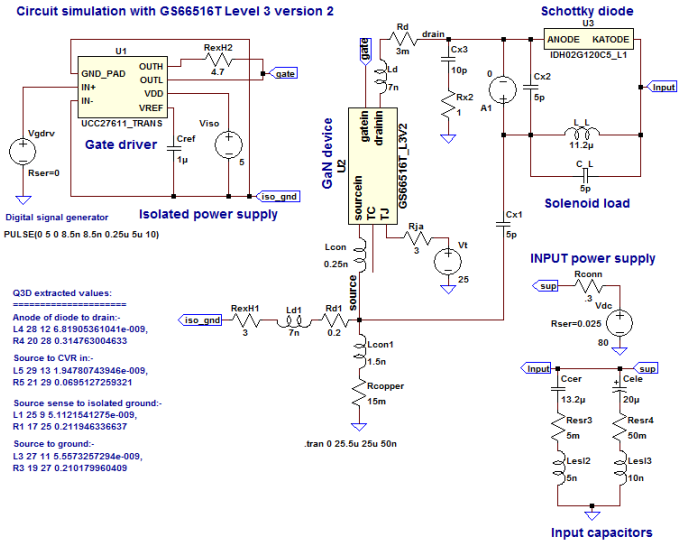

Fig. 10. LTSpice meta-model of double-pulse GaN HEMT circuit without mounting a CVR

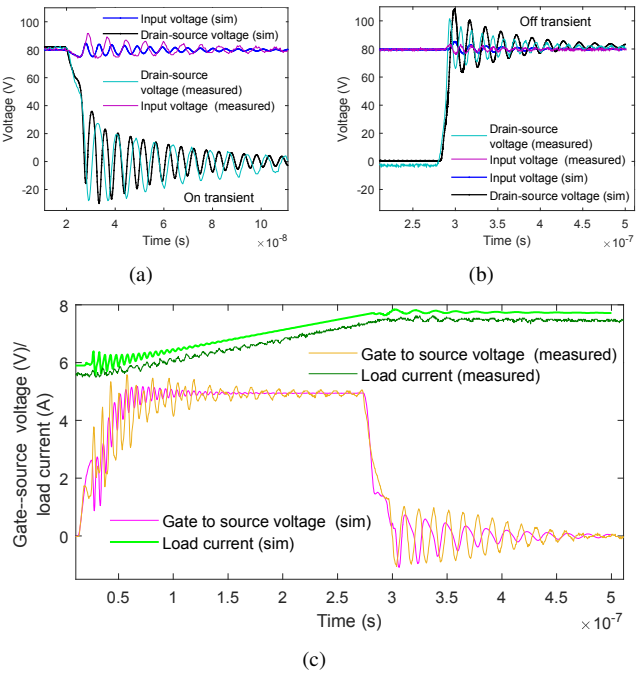

Fig. 11. Comparison of results of the *case 2* SPICE simulation model. No current sensing resistor is implemented in this circuit.

Figures 12(a) and (b) illustrate a comparison of CVR-based current measurements in *case 1* with the simulation results of *case 2*. Both load and the drain currents are compared during on and off transients. As seen in the figure, the oscillations of the measured drain current during the on-transients are higher compared to a predicted results of *case 2*. This confirms that measuring drain current using a CVR adds error to the readings. Besides, low frequency oscillations in the measurements can lead to inaccurate estimations of power dissipation in the

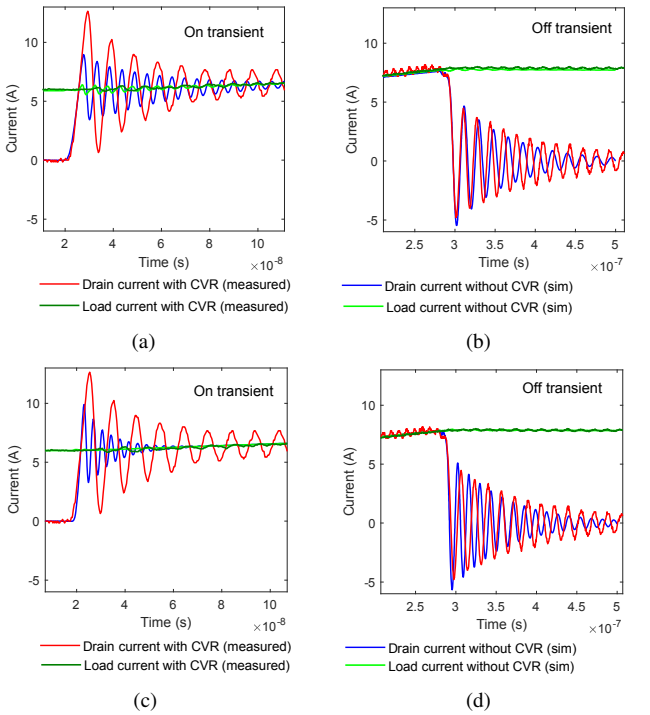

Fig. 12. A comparison of measured drain current of *case 1* and the SPICE simulation models: (a) and (b) compare the results with the simulation model of *case 2*. In the simulation, the drain-current obtained at the drain terminal. For the comparisons of (c) and (d), the parasitics in PCB traces are ignored in the simulation model.

device.

For further investigations, a simulation model was designed with an ideal PCB layout. In this model, the parasitic components related to the PCB traces considered in Fig. 9(a) were ignored. The results of the simulation were used to demonstrate the layout parasitic effect as seen in Fig.s 12(c) and 12(d) in blue traces. In the ideal case of this design, the drain current waveform would oscillate a minimum of 60 ns during on-transients whereas in *case 2* it is approximately 100 ns (see Fig. 12(a)). A maximum of 40% oscillation period can be reduced by eliminating the parasitic components in the PCB layout. However, compared to both designs the error of drain current through a CVR is high. Although it seems to offer the best current measurement performance, the CVR introduces unavoidable perturbations to the measurements.

V. Conclusion

A study of CVR-based drain current measurement is performed. By implementing a fairly precise simulation model, the effect of adding CVR in the power path is observed. The *case 2* SPICE simulations achieved a fair agreement of experiment results. The model was able to predict drain current even during transients. Therefore, the PCB without CVR can be consider as more accurate, and may use for analysis of the converter operation. As seen in the results, more perturbations in readings can be reduced by optimizing the PCB design to reduce the copper-track related parasitics. According to the results comparisons, CVR-based measurements introduce considerably oscillations during the on-transients. Despite of slight difference in the period of oscillations, the CVR can measure the drain current during off-transients more accurately.

References

[1] B. Mammano, "Current sensing solutions for power supply designers". In Proc. TI Power Supply Design Sem. 1997.

[2] S. Ziegler, R.C. Woodward, H.H.C. Iu, and L.J. Borle, "Current sensing techniques: A review." *IEEE Sensors Journal*, vol. 9, no. 4, pp.354-376, 2009.

[3] B. Strzalkowski, J. Sorensen, "Challenges and solutions of high-side current and of phase current measurement", presented at ECPE Workshop, Hamburg, Germany, Oct 17th, 2017.

[4] J. Schiffner, "Shunt resistors for precision current measurement, presented at ECPE Workshop", Hamburg, Germany, Oct 17th, 2017.

[5] M. Adelmund, C. Bodeker and N. Kaminski, May. "Optimisation of Shunt Resistors for Fast Transients" In PCIM Europe 2016; International Exhibition and Conference for Power Electronics, Intelligent Motion, Renewable Energy and Energy Management, 2016, pp. 1-8.

[6] C. Xiao, L. Zhao, et.al, "An overview of integratable current sensor technologies", in *Industry Applications Conference, 38th IAS Annual Meeting*, October 2003, pp. 1251-1258.

[7] Billmann, "Dimensioning of a proper coaxial shunt type", presented at ECPE Workshop, Hamburg, Germany, Oct 17th, 2017.

[8] C.Hewson and J. Aberdeen, "Wide-Bandwith Rogowski based Measurement in the Lab", presented at ECPE Workshop, Hamburg, Germany, Oct 17th, 2017.

[9] M. Denk and S. Hain, Case Study - "High Bandwith and Minimal Invasive Current Measurement", presented at ECPE Workshop, Hamburg, Germany, Oct 17th, 2017.

[10] J. Lenz and S. Edelstein, 2006. "Magnetic sensors and their applications" *IEEE Sensors Journal*, vol. 6, no.3, pp.631-649.

[11] Vishay, "Medium Power Planar Transformer 1 kW to 3 kW", PLA51 datasheet, 2017 [Revision: 8 Feb. 2017]

[12] R. Slatter and M. Kramb, "High bandwidth, highly integrated current sensors for high power density electromobility applications", In Proc. Power Electronics, Machines and Drives (PEMD 2016), 8th IET International Conference, April 2016, pp. 1-6.

[13] R. Slatter, "High accuracy, high bandwidth magnetoresistive current sensors for spacecraft power electronics", In Proc. 2015 17th European Conference on Power Electronics and Applications (EPE'15 ECCE-Europe), Sept.2015, pp. 1-10.

[14] A. Bouzourene, T. Bensalah, L. Cima and A. Couderette, "Investigation of Neel Effect technology for current sensors in next-generation aeronautical applications", In Proc. 2011-14th Power Electronics and Applications (EPE 2011) Conference, Aug. 2011 pp. 1-10.

[15] T&M Research Products, Inc., "Series SDN-414", SDN-414-025 specifications.

[16] GaN Systems Inc.: "LTspice Model User Guide" [available online] https://gansystems.com/wp-content/uploads/2018/05/LTspice-Model-User-Guide.pdf